Method of lines solutions of the extended Boussinesq equations

S. Hamdi [a,*] W. H. Enright [b] Y. Ouellet [c] W. E. Schiesser [d]

[a] *Baird & Associates Coastal Engineers, 1145 Hunt Club Road, Suite 500 Ottawa, Ontario, Canada, K1V 0Y3*

[b] *Department of Computer Science, University of Toronto, 10 King's College Road, Toronto, Canada, M5S 3G4*

[c] *Département de Génie Civil, Université Laval, Québec, Canada G1K 7P4*

[d] *Mathematics and Engineering, Lehigh University, Bethlehem, PA 18015 USA*

Abstract

A numerical solution procedure based on the method of lines for solving the Nwogu's one-dimensional extended Boussinesq equations is presented. The numerical scheme is accurate up to fifth order in time and fourth-order accurate in space, thus reducing all truncation errors to a level smaller than the dispersive terms retained by most extended Boussinesq models. Exact solitary wave solutions and invariants of motions recently derived by the authors are used to specify initial data for the incident solitary waves in the numerical model of Nwogu and for the verification of the associated computed solutions. The invariants of motions and several error measures are monitored in order to assess the conservative properties and the accuracy of the numerical scheme. The proposed method of lines solution procedure is general and can be easily modified to solve a wide range of Boussinesq-like equations in coastal engineering.

Key words: Method of lines, Boussniesq equations, nonlinearity, dispersion, solitary waves solutions, invariants of motion.

1 Introduction

Boussinesq-type equations are derived by integrating the three-dimensional Euler equations through the depth using a polynomial approximation of the vertical profile of the

* Supported by the Department of Computer Science, University of Toronto and the Natural Science and Engineering Research Council of Canada.

Email address: samir.hamdi@utoronto.ca (S. Hamdi).

velocity field, thereby reducing the three-dimensional problem to an equivalent (within the approximation made) two-dimensional problem and making them relatively efficient to solve numerically. In this regard, the Boussinesq equations are good alternative to Euler equations and enable simulations in domains of much larger extents. The first such system of equations for water of varying depth was derived by Peregrine (1967), which are now often called the standard Boussinesq equations and which include the lowest order effects of nonlinearity and frequency dispersion. The standard Boussinesq equations have been used extensively to model accurately wave evolution in nearshore zone. They can be used, for example, to describe the nonlinear transformation of surface waves in shallow water due to the effects of shoaling, refraction, diffraction, and reflection.

A major limitation of the standard Boussinesq equations is their restricted range of applicability, which is confined to relatively shallow water depths such that the simplified vertical velocity distribution in the mathematical model remains a valid approximation. It was shown that the errors in the modeled linear dispersion relations in the commonly used forms of the Boussinesq equations increase with increasing depth. In recent years, efforts have been made by a number of researchers to extend the range of applicability of the Boussinesq system to deeper water by improving the dispersion characteristics of the equation (Madsen et al. [7,8]; Nwogu [9]; Beji et al. [1]; Lynett et al [6]).

Although most extended Boussinesq systems of equations have equivalent linearized dispersion characteristics, similar shoaling properties and formally comparable accuracy, the extended Boussinesq equations proposed by Nwogu [9] have recently generated the most interest. These equations are obtained through a consistent derivation from the continuity and Euler equation of motion. Compared to similar models derived by Madsen [7] and Beji [1], the Nwogu model is easier to solve numerically in the case of variable depth [16].

Several numerical schemes have been proposed to solve the Nwogu's extended Boussinesq equations. Wei and Kirby [17] developed a numerical code, that is fourth-order accurate in time and space, for solving these equations. The numerical solutions of Wei and Kirby [17] are more accurate than those obtained by Nwogu [9] since their solution technique is based on a higher order finite difference discretization scheme coupled with a high-order predictor-corrector time integration method. Their numerical scheme reduces the truncation errors to a level smaller than the dispersive terms retained by Nwogu's Boussinesq equations. It was shown that in most Boussinesq systems the truncation errors of a low-order approximation in space could contaminate the numerical accuracy because they have the same mathematical form as the dispersive terms appearing in the model [17].

Recently, Walkley and Berzins [16] implemented a high order accurate method of lines (MOL) solution using a Galerkin finite element spatial discretization technique coupled with the adaptive time integration package SPRINT [15]. Their spatial discretization method cannot be applied directly to the extended Boussinesq system of equation due to the presence of the third-order spatial derivatives U_{xxx}. To overcome this difficulty, they have rewritten the equations in a lower order form, suitable for a linear finite element approximation, by introducing an auxiliary algebraic equation which increases the computational effort and may reduce the efficiency of the numerical scheme.

Both, Wei and Kirby [17] and Walkley and Berzins [16] investigated solitary wave propagation over a long and flat bottom in order to assess the accuracy, the stability and the conservation properties of their numerical schemes. Wei and Kirby [17] applied this important test problem for which they derived approximate analytical solitary wave solutions following a procedure described in Schember [11]. These approximate analytical solutions are used to specify initial data for the incident waves in their numerical models and also to assess the accuracy of the associated computed solution.

The numerical results obtained by Wei and Kirby [17] for these test problems indicate that a slightly higher amplitude solitary wave is formed together with a small dispersive tail lagging behind, compared to the approximate analytical solution [11,17]. The wave profiles also show that the amplitude of the tail and the initial deviation in solitary-wave height both increase with increasing initial wave height. They also observed that the numerically predicted phase speed is somewhat smaller than the analytically predicted one, and that the difference increases with increasing wave height. Such discrepancies are explained by the fact that the analytical solutions are only an approximation of the closed-form solutions and does not correspond exactly to a solitary waveform as predicted by the model.

Walkley and Berzins [16] reported very similar results to those obtained by Wei and Kirby [17] for the same solitary wave test problem. They have also observed that there is an identical slight phase error in the numerical results and a small dispersive tail. They concluded that the analytical solution [11,17] is only an approximation and therefore exact agreement is unlikely.

In this paper we present a method of lines solution of the Nwogu's one-dimensional extended Boussinesq equations using the time integrator `DASSL` [10], which is based on a variable time step and variable order backward-differentiation formulae (BDF). The numerical scheme is accurate up to the fifth order in time and fourth-order accurate in space, thus reducing all truncation errors to a level smaller than the dispersive terms retained by most extended Boussinesq models. Unlike the MOL proposed by Walkley and Berzins [16] which requires the introduction of an auxiliary algebraic equation that may reduce the efficiency of the numerical scheme, our MOL solution of the extended Boussinesq equations does not require any transformation or any manipulation of the model equations. Our MOL implementation has the advantage of a close resemblance of the MOL programming of the the PDE with the PDE itself and uses a simple grid point ordering for bandwidth reduction of the Jacobian matrix of the integrator `DASSL`. This MOL implementation leads to efficient solutions of the Boussinesq system. The nonlinear terms and dispersive terms are accommodated easily using quality library routines [3,10,12–14].

Exact solitary wave solutions and invariants of motions recently derived by the authors [5] are used to specify initial data for the incident solitary waves in the numerical model of Nwogu and for the verification of the associated computed solution. These new exact solitary wave solutions are used instead of the approximate solutions to overcome the problems reported by Wei and Kirby [17] and Walkley and Berzins [16]. The invariants of motions and several error measures are monitored in order to assess the conservative properties and the accuracy of the numerical scheme.

2 The extended Boussinesq equations

In the case of wave propagation in the one-dimensional (1D) horizontal direction with constant depth, the extended Boussinesq equations derived by Nwogu [9] and considered by Wei et al. [17] in their numerical code, reduce to the following:

$$\eta_t + hu_x + (\eta u)_x + (\alpha + 1/3)h^3 u_{xxx} = 0 \tag{1}$$

$$u_t + g\eta_x + uu_x + \alpha h^2 u_{txx} = 0 \tag{2}$$

with

$$\alpha = \frac{1}{2}\left(\frac{z_\alpha}{h}\right)^2 + \frac{z_\alpha}{h} \tag{3}$$

where η = surface elevation; h = local water depth; $u = u(x,t)$ horizontal velocity at an arbitrary depth z_α ; and g = the gravitational acceleration. These equations are statements of conservation of mass and momentum, respectively.

Two important length scales are the characteristic water depth h_0 in the vertical direction and a typical wavelength l in the horizontal direction. The following non-dimensional independent variables can be defined:

$$x = \frac{\tilde{x}}{l}, \qquad z = \frac{\tilde{z}}{h_0}, \qquad t = \frac{\sqrt{gh_0}}{l}\,\tilde{t}\,. \tag{4}$$

The tildes are used to connote dimensional variables as in the set of equations (1) and (2). For effects related to the motion of the free water surface, the typical wave amplitude a_0 is also important. The following non-dimensional dependent variables can also be defined:

$$u = \frac{h_0}{a_0\sqrt{gh_0}}\,\tilde{u}, \qquad \eta = \frac{\tilde{\eta}}{a_0}, \qquad h = \frac{\tilde{h}}{h_0}\,. \tag{5}$$

Using the transformation (4) and (5), the Nwogu's set of equations (1) and (2) are rewritten in dimensionless form as follows

$$\eta_t + u_x + \delta(\eta u)_x + \mu^2(\alpha + 1/3)u_{xxx} = 0 \tag{6}$$

$$u_t + \eta_x + \delta u u_x + \mu^2 \alpha u_{txx} = 0 \tag{7}$$

The dimensionless parameters $\delta = a_0/h_0$ and $\mu = h_0/l$ are measures of nonlinearity and frequency dispersion, respectively, and are assumed to be small ($\delta << 1$ and $\mu << 1$). The parameter α reduces to

$$\alpha = \frac{1}{2}(z_\alpha)^2 + z_\alpha \quad . \tag{8}$$

2.1 Exact solitary wave solutions

The authors [5] recently derived exact solitary wave solution for the extended Boussinesq equations of Nwogu using `MAPLE` software. The solitary wave solution for the free surface elevation $\eta(x,t)$ is in the form

$$\eta(x,t) = \eta_0 \,\mathrm{sech}^2\left(\kappa(x - x_0 - Ct)\right)\,. \tag{9}$$

which corresponds to a single hump of amplitude η_0 initially centered at x_0. This solitary wave has a wave number κ and travels without change of shape at a steady speed C.

The solitary wave solution for the horizontal velocity $u(x,t)$ is given by

$$u(x,t) = A\,\eta_0\,\mathrm{sech}^2\left(\kappa(x - x_0 - Ct)\right)\ , \tag{10}$$

where

$$A = \pm\sqrt{\frac{3}{\delta\,\eta_0 + 3}} = \pm 2\sqrt{\frac{\alpha}{\alpha - 1/3}}\,. \tag{11}$$

The wave speed is given by,

$$C = \frac{2 - A^2}{A} = \pm\frac{2\,\delta\,\eta_0 + 3}{\sqrt{3\,(\delta\,\eta_0 + 3)}} = \pm\frac{\alpha + 1/3}{\sqrt{\alpha(\alpha - 1/3)}}\ , \tag{12}$$

with the corresponding wave amplitude,

$$\eta_0 = \frac{3(1 - A^2)}{\delta A^2} = -\frac{1}{4}\ \frac{9\,\alpha + 1}{\alpha\,\delta}\ , \tag{13}$$

and wave number,

$$\kappa = \frac{1}{2}\sqrt{\frac{2(1 - A^2)}{\mu^2(\alpha + 1/3)A^2}} = \frac{1}{2}\sqrt{\frac{2\,\eta_0\,\delta}{3\mu^2(\alpha + 1/3)}} = \frac{\sqrt{6}}{12}\,\sqrt{\frac{9\,\alpha + 1}{(\alpha + 1/3)\,\mu^2\,(-\alpha)}}\quad . \tag{14}$$

2.2 Influence of the dispersion parameter on solitary wave profiles

The profiles of the exact solitary wave solution, for different values of the parameter μ, are shown in figure (1) for the free surface elevation $\eta(x,t)$ and the horizontal velocity $u(x,t)$ which is centered at $x_0 = 0$ and plotted at the initial time $t = 0$. The parameter μ represents the importance of the frequency dispersion and has a direct effect on the profiles of the solitary waves. From (14) it is clear that smaller values of μ will lead to larger values of the wave number κ and therefore to a reduced width of the solitary wave profile. Such solitary waves with narrow profile and steep gradients are more difficult to resolve numerically. Moreover, it is apparent from the scaled Boussinesq equations (6) and (7) that reduced values of μ lead to smaller dispersive terms $\mu^2 u_{xxx}$ and $\mu^2 u_{xxt}$. In this regard, the Boussinesq equations become challenging to solve numerically particularly when the size of the dispersive terms are reduced to the same order of magnitude as the leading truncation error terms of the underlying numerical scheme.

An appraisal of the influence of the dispersion parameter μ on the solitary wave profile suggests making the following change of variables:

$$\hat{x} = \frac{x}{\beta} \quad \text{and} \quad \hat{t} = \frac{t}{\beta} \tag{15}$$

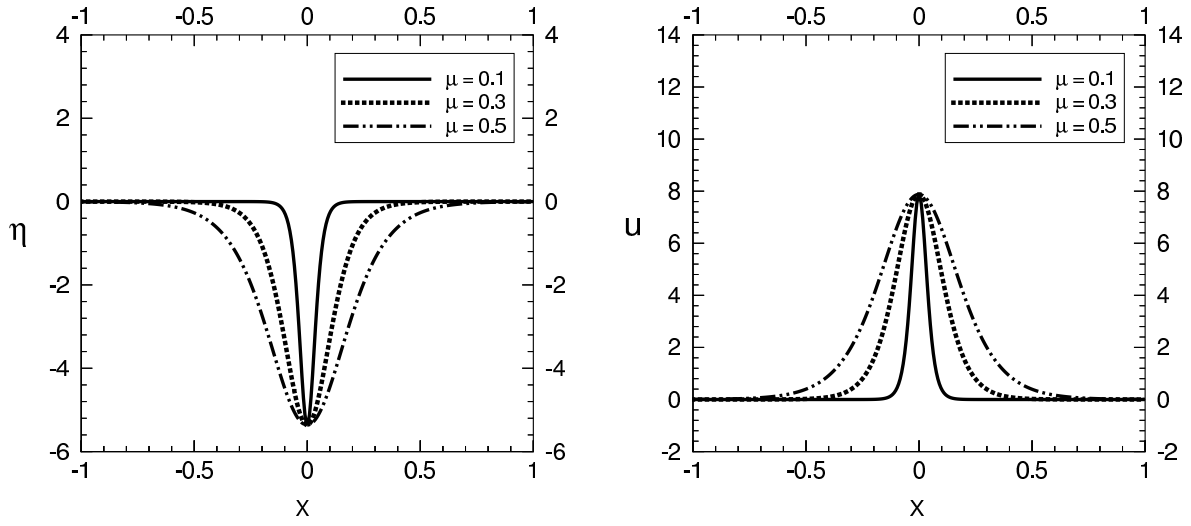

Fig. 1. Influence of the dispersion parameter μ on solitary wave profiles for $\delta = 0.3$ and $\alpha = -0.39$.

Using the new variables, (6) and (7) can be rewritten in the form,

$$\eta_{\hat{t}} + u_{\hat{x}} + \delta(\eta u)_{\hat{x}} + \hat{\mu}^2\,(\alpha + 1/3) u_{\hat{x}\hat{x}\hat{x}} = 0 \tag{16}$$

$$u_{\hat{t}} + \eta_{\hat{x}} + \delta u u_{\hat{x}} + \hat{\mu}^2\,\alpha u_{\hat{t}\hat{x}\hat{x}} = 0 \tag{17}$$

where $\hat{\mu} = \mu/\beta$. From (14), we obtain the corresponding wave number of the solitary wave solution,

$$\hat{\kappa} = \beta\kappa = \frac{\sqrt{6}}{12}\sqrt{\frac{9\,\alpha + 1}{(\alpha + 1/3)\,(\frac{\mu}{\beta})^2\,(-\alpha)}} \tag{18}$$

The exact solitary wave solution expressed in terms of variables $(\hat{x}, \hat{t}\,)$ or (x, t) are then given by,

$$\eta(\hat{x}, \hat{t}\,) = \eta_0\,\mathrm{sech}^2\left(\hat{\kappa}(\hat{x} - \hat{x}_0 - C\,\hat{t}\,)\right) = \eta_0\,\mathrm{sech}^2\left(\kappa(x - x_0 - Ct)\right) = \eta(x, t) \tag{19}$$

and

$$u(\hat{x}, \hat{t}\,) = A\,\eta_0\,\mathrm{sech}^2\left(\hat{\kappa}(\hat{x} - \hat{x}_0 - C\,\hat{t}\,)\right) = A\,\eta_0\,\mathrm{sech}^2\left(\kappa(x - x_0 - Ct)\right) = A\,\eta(x, t) \tag{20}$$

It follows that the scaling factor β controls the width of the solitary wave profile in the new variables $(\hat{x}, \hat{t}\,)$.

2.3 Invariants of motion of solitary wave solutions

The authors [5] recently derived exact expressions for four constants of motion corresponding to the solitary wave solutions (9) and (10) using `MAPLE` software. In this section, we present a brief review of the derivation of these analytical expressions.

The Nwogu system of equations seems to have at least two conservation laws.

The first invariant of motion corresponds to the conservation of mass,

$$I_1 = \int_{-\infty}^{+\infty} \eta(x,t)\,\mathrm{d}x\,. \tag{21}$$

Using the analytical expression (9) for the exact solitary wave solution $\eta(x,t)$, we obtain,

$$I_1 = 2\,\frac{\eta_0}{\kappa}\,. \tag{22}$$

Substituting (13) and (14) into (22), it follows that,

$$I_1 = \frac{\sqrt{6}}{\delta\,\alpha}\,\sqrt{-\alpha\,\mu^2\,(\alpha+1/3)\,(9\,\alpha+1)}\,. \tag{23}$$

Another invariant of motion is the integral,

$$I_2 = \int_{-\infty}^{+\infty} u(x,t)\,\mathrm{d}x\,. \tag{24}$$

Substituting the expression of the solitary wave solution (10) for the horizontal velocity in the above integral we obtain,

$$I_2 = A\,I_1 = \frac{2\,\eta_0}{\kappa}\,A\,, \tag{25}$$

and, in explicit form,

$$I_2 = \pm\frac{2\,\eta_0}{\kappa}\,\sqrt{\frac{3}{\delta\,\eta_0+3}} = \pm\frac{2}{\delta}\,\sqrt{\frac{-6\,\mu^2\,(\alpha+1/3)\,(9\,\alpha+1)}{\alpha-1/3}}\,. \tag{26}$$

The impulse functional given by,

$$I_3 = I(\eta,u) = \int_{-\infty}^{+\infty} \Big(\eta(x,t)u(x,t) - \alpha\,\mu^2\,\eta_x(x,t)\,u_x(x,t)\Big)\;\mathrm{d}x\,, \tag{27}$$

is also a constant of motion for the solitary wave solutions (9) and (10), which can be expressed explicitly as

$$\begin{aligned} I_3 &= A\int_{-\infty}^{+\infty}\left(\eta^2 - \alpha\mu^2\eta_x^2\right)\,\mathrm{d}x \\ &= \frac{4}{15}\,\frac{\eta_0^2\,A(5-4\alpha\mu^2\kappa^2)}{\kappa} \\ &= \pm\frac{(39\,\alpha+11)}{10\,\alpha\delta^2}\,\sqrt{\frac{2\mu^2}{3}\,\frac{(1+9\,\alpha)^3}{(1-9\,\alpha^2)}}\,. \end{aligned} \tag{28}$$

Because dissipation is ignored in the derivation of the Nwogu-Boussinesq model,we can define a Hamiltonian-like form for the system (6) and (7),

$$I_4 = H(\eta,u) = \int_{-\infty}^{+\infty}\left(\mu^2\,(\alpha+1/3)\,u_x^2 - \eta^2 - u^2 - \delta\,u^2\eta\right)\,\mathrm{d}x\quad. \tag{29}$$

This integral is not a Hamiltonian but it is a constant of motion for the solitary wave solutions (9) and (10), which to say that the functional H satisfies,

$$H(\eta(x,t),u(x,t)) = H(\eta(x,0),u(x,0)) \quad . \tag{30}$$

Substituting (9) and (10) for $\eta(x,t)$ and $u(x,t)$ respectively in (29), we obtain,

$$I_4 = \frac{4}{45}\,\frac{\eta_0^2\,(12\alpha\,\mu^2\,A^2\,\kappa^2 + 4\mu^2\,A^2\kappa^2 - 12\,\delta\,A^2\eta_0 - 15A^2 - 15)}{\kappa} \quad , \tag{31}$$

which can be written in explicit form,

$$I_4 = \frac{1}{2}\,\frac{(\alpha+1)\,\sqrt{(-2\,\alpha)\,(3\,\alpha+1)\,(9\,\alpha+1)^3\,\mu^2}}{(3\,\alpha-1)\,\alpha^2\,\delta^2} \quad . \tag{32}$$

3 Method of lines solution of the Boussinesq system

3.1 Numerical solution procedure

A description of the method of lines (MOL) solution of the Boussinesq equations, is given in this section. The method of lines consists in essence of numerically integrating this system of partial differential equations (PDEs) forward in time to advance the solutions $\eta(x,t)$ and $u(x,t)$ at every node of a spatial grid, with $\eta(x,t)$ and $u(x,t)$ specified at each grid node at some initial time (e.g., $t=0$) and boundary conditions applied at each time step to specify $\eta(x,t)$ and $u(x,t)$ at the two edge nodes of the grid. The solution of the Boussinesq equations on a uniform grid or nonuniform grid requires discretizations of the spatial derivative terms η_x, u_x, u_{xxx} and u_{xxt} , and these discretizations can lead to a large set of stiff and implicit ordinary differential equations (ODEs). These ODEs are integrated forward in time using an advanced ODE solver.

To help describe the solution procedure more concisely the Boussinesq equations are written in functional notation as

$$f(\eta_t, u_t, \eta_x, u_x, u_{xxx}, u_{xxt}) = 0, \qquad x_{\mathrm{L}} \le x \le x_{\mathrm{U}} \qquad \text{and} \qquad 0 \le t \le t_U \tag{33}$$

in which u and η are the dependent variables, x and t are the independent variables, and x_{L} and x_{U} correspond to the lower and upper limits or boundaries on x. As subscripts, x and t denote partial derivatives. Suitable boundary conditions at x_{L} and x_{U} are generally required to determine the solution numerically. However, for most problems in which wave propagation occurs well inside the boundaries, the solution is negligible at or outside the boundaries during the time span of interest. Consequently, Dirichlet boundary conditions at the lower and upper ends of the interval $[x_L, x_U]$, given by $u(x_L,t) = u_L$ and $u(x_U,t) = u_U$, are used.

The numerical discretizations of the spatial derivatives $(\eta_x, u_x, u_{xxx}, u_{xxt})$ in the Boussinesq equations are obtained using centered fourth order finite-difference approximations

for all terms. All spatial discretizations in this study were generated systematically with the versatile algorithm called `WEIGHTS` from Fornberg [3] which can be used for both uniform and nonuniform grids.

The direct spatial discretization of the Boussinesq system of equations on a grid of n nodes given by $\underline{x} = [x_1, x_2, \cdots, x_n]$ produces a set of $2n$ ODEs that can be expressed in vector form as,

$$\underline{f}\left(\underline{y}, \frac{\mathrm{d}\underline{y}}{\mathrm{d}t}, t\right) = \underline{0}, \tag{34}$$

and the initial conditions can be expressed likewise as

$$\underline{f}\left(\underline{y}\big|_{t_0}, \left.\frac{\mathrm{d}\underline{y}}{\mathrm{d}t}\right|_{t_0}, t_0\right) = \underline{0}, \tag{35}$$

where,

$$\underline{y} = [\eta_1, \eta_2, \cdots, \eta_n; u_1, u_2, \cdots, u_n] \tag{36}$$

$$\mathrm{d}\underline{y}/\mathrm{d}t = [\mathrm{d}\eta_1/\mathrm{d}t, \mathrm{d}\eta_2/\mathrm{d}t, \cdots, \mathrm{d}\eta_n/\mathrm{d}t; \mathrm{d}u_1/\mathrm{d}t, \mathrm{d}u_2/\mathrm{d}t, \cdots, \mathrm{d}u_n/\mathrm{d}t] \tag{37}$$

$$\underline{f} = [f_1, f_2, \cdots, f_n; f_{n+1}, f_{n+2}, \cdots, f_{2n}] \tag{38}$$

This semi-discretization of the Boussinesq equations on a spatial grid, which involves the mixed space and time derivatives u_{xxt}, results in an implicit set of ODEs because the vector of derivatives $\mathrm{d}\underline{u}/\mathrm{d}t$ is defined implicitly through the vector function $\underline{f}$. In this regard, the MOL solution of the Boussinesq equations is very similar to the MOL solution of the equal width wave equation $u_t + uu_x - \mu u_{xxt} = 0$. For a detailed discussion of a host of issues surrounding nonlinear dispersive wave equations involving mixed space and time derivatives u_{xxt}, we refer the reader to the study of Hamdi et al. [4] and the references therein.

For problems involving solitary wave propagation, the boundary conditions are often algebraic in form and do not contain any derivative terms. Therefore some of the functions f_i in (38) are algebraic equations. In this case, (34) is a set of differential algebraic equations (DAEs).

The implicit DAE system given by equation (34) is integrated numerically in time in this study using an advanced DAE solver, `DASSL` developed by Petzold [10]. This versatile solver has special features for solving stiff DAEs. It can be used to integrate in time either ODEs or DAEs, such that different problems governed by the Boussinesq equations which involve differential or algebraic boundary conditions can be solved easily with minor computer-code modifications. In previous numerical studies of the Boussinesq equations the time integration has usually been performed with low order methods which can result in significant truncation errors that produce non-physical dispersion and therefore contaminate the mathematical model (see Walkley and Berzins [16]). In this study high accuracy is achieved by making use of the solver `DASSL` which is based on variable time step and variable order backward-differentiation formulae (BDF).

The local errors in the solution $\underline{y}$ over each time step are controlled in `DASSL` by varying both the order of the BDF method and the time step in order to achieve high accuracy and stability in the integration. The local errors are controlled by the user by setting small

values for relative and absolute tolerances ATOL and RTOL. In this study, tight tolerances (such as ATOL=RTOL $= 10^{-10}$) are chosen to reduce the time integration errors so that only spatial truncation errors dominate. The solver DASSL normally requires the initial derivatives $\mathrm{d}\underline{y_0}/\mathrm{d}t$ and a consistent set of initial conditions. In this study the initial derivatives are computed automatically in DASSL using the initial solution $\underline{y_0}$ and requiring that the system $\underline{f}\left(\underline{y_0}, \mathrm{d}\underline{y_0}/\mathrm{d}t, t_0\right) = \underline{0}$ be satisfied.

In DASSL an approximate Jacobian matrix of the DAEs is computed internally using finite differences. In the case of the Boussinesq system of equations which are actually a set of two simultaneous PDEs, the Jacobian matrix is not banded and has outlying diagonals due to the coupling between the PDEs. The use of an implicit banded DAE integrator like DASSL with full (dense) Jacobian matrix option is computationally inefficient because a large number of arithmetic operations would be required to produce the numerical solution. In this study we implement a bandwidth reduction of the Jacobian matrix by using a simple grid point ordering $\underline{y} = [\eta_1, u_1, \eta_2, u_2, \cdots, \eta_n, u_n]$ which clearly changes the structure of the Jacobian and leads to substantial reductions in the computation for the DAE solution (see for example Schiesser [14] for implementation details of grid point ordering and Jacobian bandwidth reduction in DASSL). Option 6 for banded Jacobian matrix of the DAE system is then selected (INFO(6)=1). The upper and lower half bandwidths, ML and MU, are each set to 10. The total bandwidth of ML+MU+1=21 is adequate to accommodate all of the nonzero elements of the Jacobian matrix for the fourth order approximations that we use for all the spatial derivatives in the Boussinesq system of equations.

3.2 Numerical results and discussion

The Boussinesq system of equations are solved in this section to predict the motion of a single solitary wave in space and time. This problem is solved for the parameters $\hat{\mu} = 0.2$, $\delta = 0.2$, $\alpha = -0.39$ and $\beta = 50$ using the method of lines that we described previously. The exact solitary wave solutions for this problem were derived in the previous sections and given by (9) and (10). The proportionality coefficient A, the wave speed C, the wave peak amplitude η_0 and the wave number κ are determined from (11), (12), (13) and (14), respectively, which depend only on the three parameters $\hat{\mu}$, δ and α of the non dimensional Boussinesq equations. Several exact and numerical results are compared for this benchmark problem to assess various parts of the solution procedure. The initial conditions for the numerical computations are determined from the exact solution at time $t = 0$ on the interval $[x_L = -60, x_U = 100]$. The wave is centered at $x_0 = 30$ at $t = 0$. The numerical solution is computed for times varying from $t = 0$ to 200 with the number of nodes varying from 500 to 4000. During the time interval 0 to 200 the solitary wave is always far from the grid boundaries, so the Dirichlet boundary conditions $u(x_L, t) = u_L = 0$ and $u(x_U, t) = u_U = 0$ are applied, because they are sufficiently accurate for the current problem.

Numerical results from the MOL solution of the Boussinesq equations are given first in the form of a time-distance diagrams in figures (2) and (3) for the free surface elevation η and horizontal velocity u, respectively. A close observation shows that the single

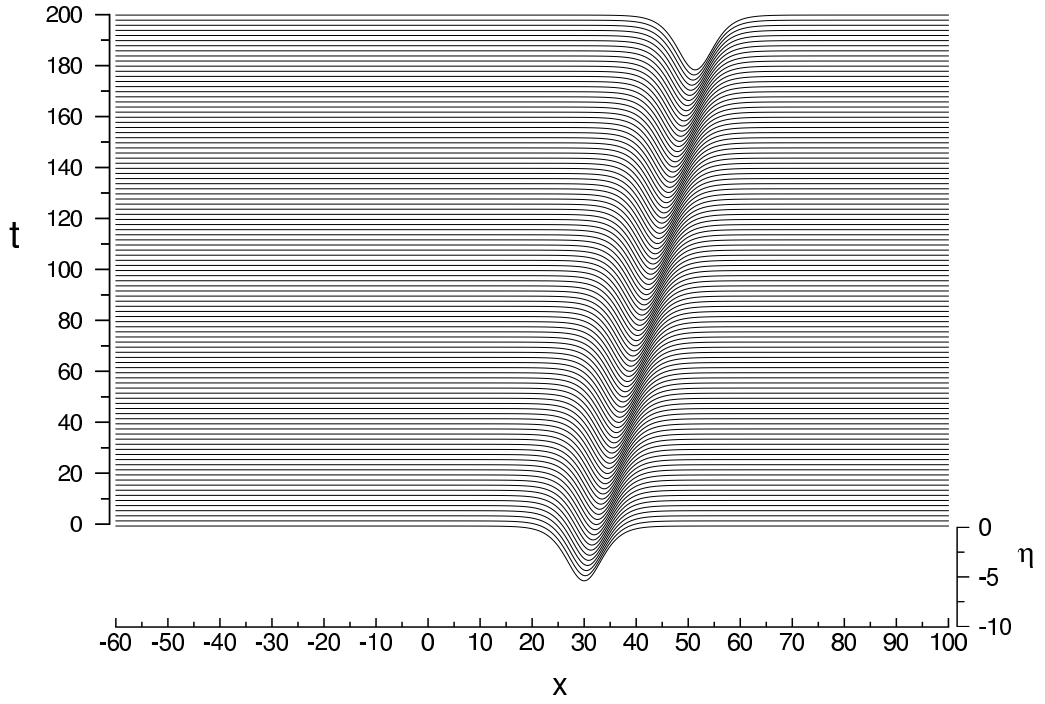

Fig. 2. Solitary wave solution $\eta(x,t)$.

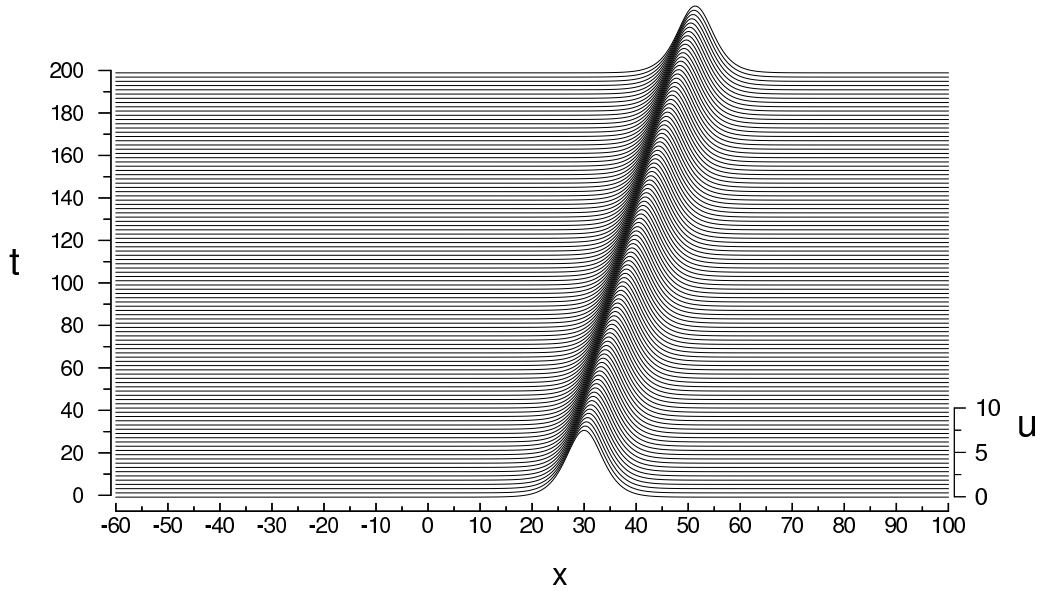

Fig. 3. Solitary wave solution $u(x,t)$.

solitary wave travels with a constant speed, peak amplitude, and shape. The numerical solutions $\eta(x_i,t_j)$ and $u(x_i,t_j)$ are in close agreement with the exact solution, if the grid nodes are sufficiently numerous, such that the exact and numerical solutions overlap and are not readily distinguishable in figure (4).

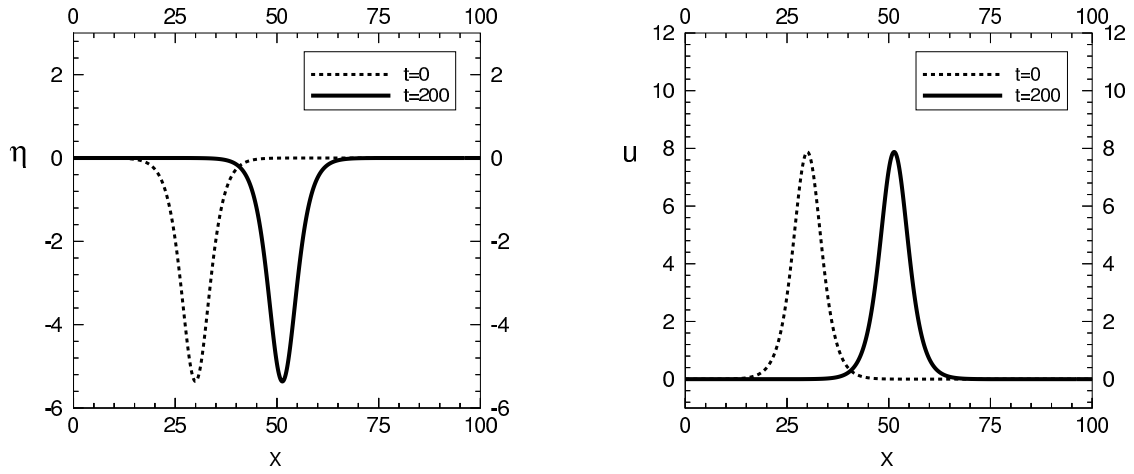

Fig. 4. Solitary wave profiles at $t = 0$ and $t = 200$.

However, the accuracy cannot be easily determined quantitatively from the results in these figures, so other results and error measures are now introduced.

Error norms have been computed for the current problem because the exact solution is known. We use the error norm L_2, which is defined by

$$L_2 = \left[\frac{1}{x_U - x_L} \sum_{i=1}^{n-1} \frac{1}{2} \left(x_{i+1} - x_i \right) \left(\left\{ y_i^{\text{exact}} - y_i^{\text{num}} \right\}^2 + \left\{ y_{i+1}^{\text{exact}} - y_{i+1}^{\text{num}} \right\}^2 \right) \right]^{1/2}, \tag{39}$$

and which can be used for both uniform or non uniform meshes. The variable y_i denotes the dependent variables $\eta(x_i, t_j)$ or $u(x_i, t_j)$ whereas y_i^{exact} and y_i^{num} represent the exact and numerical solutions for the variables $\eta(x_i, t_j)$ and $u(x_i, t_j)$ at the ith node x_i. We also use the norm $L_\infty = \|u^{\text{exact}} - u^{\text{num}}\|_\infty$, defined as

$$L_\infty \ = \max_i \left| u_i^{\text{exact}} - u_i^{\text{num}} \right| \tag{40}$$

Results for these error norms for 500 nodes and varying times from $t = 0$ to 100 are summarized in Tables (1). Both errors increase slightly with time integration but remain very small and bounded. Such tabulated results illustrate clearly the advantage of using error measures to assess the accuracy of the numerical solutions compared to qualitative plots of the solution profiles as shown in figures (2), (3) and (4).

We use the exact solitary wave solutions to demonstrate that the error from the spatial discretization is of order $\triangle x^4$. This is accomplished by setting very small values for relative and absolute tolerances `ATOL` and `RTOL` in `DASSL` and varying the step size in space. We took `ATOL=RTOL` $= 10^{-12}$ and $\triangle x = 1.28/2^m$, for $m = 1, 2, 3, 4, 5$, and compared the numerically generated approximation with the exact solution at $t = 1$ for each value of m. The max-norms for the errors in η and u, which are denoted by L_∞^η and L_∞^u, respectively, were computed. The outcome for different number of nodes ($n = 500, 1000, 2000, 4000$) is shown in Table (2). The second column in Table (2) corresponds to the step size in space. Increasing m by 1 halves the grid size, which results in the number of mesh points being

Table 1
Error norms L_2 and L_∞.

Time	L_2^η	L_∞^η	L_2^u	L_∞^u
20	0.04630	0.0013	0.0680	0.00025
40	0.04633	0.0013	0.0680	0.00063
60	0.04637	0.0014	0.0681	0.00105
80	0.04642	0.0014	0.0682	0.00149
100	0.04647	0.0017	0.0682	0.00193

$\alpha = -0.39$, $\delta = 0.3$, $\hat{\mu} = 0.2$, $\beta = 50$, $\triangle x = 0.32$, $n = 500$,

$\texttt{ATOL} = \texttt{RTOL} = 10^{-9}$, $C = 0.106690591669$, $A = -1.46856461473$

Table 2
Numerical validation of the fourth order accuracy ($\triangle x^4$) of the spatial discretization.

n	m	L_∞^η	$[L_\infty^\eta(m-1)]\,/\,[L_\infty^\eta(m)]$	L_∞^u	$[L_\infty^u(m-1)]\,/\,[L_\infty^u(m)]$
250	1	0.748×10^{-2}		0.131×10^{-3}	
500	2	0.500×10^{-3}	14.96	0.863×10^{-5}	15.17
1000	3	0.320×10^{-4}	15.63	0.544×10^{-6}	15.86
2000	4	0.200×10^{-5}	16.00	0.342×10^{-7}	15.91
4000	5	0.125×10^{-6}	16.00	0.214×10^{-8}	15.98

$\alpha = -0.39$, $\delta = 0.3$, $\hat{\mu} = 0.2$, $\beta = 50$, $t = 1$, $\triangle x = 1.28/2^m$ for $m = 1, 2, 3, 4, 5$,

$\texttt{ATOL} = \texttt{RTOL} = 10^{-12}$, $C = 0.106690591669$, $A = -1.46856461473$

doubled. The third column shows the maximum absolute error L_∞^η at the mesh points. The ratio $[L_\infty^\eta(m-1)]\,/\,[L_\infty^\eta(m)]$, corresponding to grid size $\triangle x = 1.28/2^{m-1}$ and grid size $\triangle x = 1.28/2^m$ respectively, is shown in the fourth column. It appears that halving the step size in space results in the error being decreased by approximately 16 times, thereby demonstrating that the discretization error is of order $\triangle x^4$. Column 5 and 6 are similar to column 3 and 4, respectively, but for the variable u.

The exact peak amplitude for the free surface elevation η_0^{exact} and for the velocity $u_0^{\text{exact}} = A\,\eta_0$ are determined using (11) and (13). The exact trajectory in space and time of the motion of both solitary waves $\eta(x,t)$ and $u(x,t)$ is given by $x_{\eta_0}^{\text{exact}} = x_{u_0}^{\text{exact}} = 30 + C\,t$ in which the wave speed is given by (12).

The corresponding numerical values of η_0^{num}, $x_{\eta_0}^{\text{num}}$, u_0^{num}, and $x_{u_0}^{\text{num}}$ obtained from the MOL solution at time level t_j (see Table (3)), can be determined by searching through the discrete data $u(x_i, t_j)$ for the maximum values and recording their corresponding node loca-

tions. Such simple results for the peak amplitude and location are generally not accurate enough for this investigation. Instead, we first interpolate $\eta(x_i, t_j)$ and $u(x_i, t_j)$ between grid nodes using the following quintic polynomial written in a convenient symmetrical form,

$$\begin{aligned} y = \; & y_i(1-\zeta)^3(1+3\zeta+6\zeta^2) \; + \; y_{i+1}(1-\xi)^3(1+3\xi+6\xi^2) \\ & + y_x|_i(1-\zeta)^3\zeta(1+3\zeta)\Delta x_i \; - \; y_x|_{i+1}(1-\xi)^3\xi(1+3\xi)\Delta x_i \\ & + \; \frac{1}{2}y_{xx}|_i(1-\zeta)^3\zeta^2\Delta x_i^2 \quad + \quad \frac{1}{2}y_{xx}|_{i+1}(1-\xi)^3\xi^2\Delta x_i^2, \end{aligned} \tag{41}$$

where all the coefficients of the polynomial are expressed directly in terms of y and its first and second space derivatives y_x and y_{xx} which are readily available at adjacent nodes x_i and x_{i+1} from the MOL solution. In this equation the variable y denotes the dependent variables $\eta(x,t)$ or $u(x,t)$, the normalized distances $\zeta = (x - x_i)/\Delta x_i$, $\xi = 1 - \zeta$, and $\Delta x_i = x_{i+1} - x_i$.

Table 3
Peak location and maximum wave amplitude.

n	m	$x_{\eta_0}^{\text{num}}$	η_0^{num}	$x_{u_0}^{\text{num}}$	u_0^{num}
500	1	40.6649873	−5.36268433	40.6689791	7.87627379
1000	2	40.6694223	−5.36325426	40.6689791	7.87627379
2000	3	40.6690155	−5.36324890	40.6690541	7.87627589
4000	4	40.6690763	−5.36324737	40.6690590	7.87627602

$\alpha = -0.39, \quad \delta = 0.3, \quad \hat{\mu} = 0.2, \quad \beta = 50, \quad \triangle x = 0.64/2^m, \quad t = 100, \quad C = 0.1066905917,$

$A = -1.468564615, \; x^{\text{exact}} = 40.66905917, \; \eta_0^{\text{exact}} = -5.363247863, \; u_0^{\text{exact}} = 7.876276033$

The maximum (peak) amplitudes η_0^{num} and u_0^{num} and their spatial locations are obtained using a well-known iterative procedure due to Brent [2]. These numerical results are presented in Table (3) at time level $t_j = 100$ for different numbers of nodes n equal to 500, 1000, 2000 and 4000.

The corresponding relative numerical errors in the peak amplitudes and their locations are given in Table (4). These relative errors in peak amplitudes and phase are defined for both $\eta(x,t)$ and $u(x,t)$ by

$$e_{\text{amp}} = 1 - \frac{\max\limits_x \; y_{\text{peak}}^{\text{num}}(x,t)}{\max\limits_x \; y_{\text{peak}}^{\text{exact}}(x,t)} \quad \text{and} \quad e_{\text{phase}} = 1 - \frac{x_{\text{peak}}^{\text{num}}(x,t)}{x_{\text{peak}}^{\text{exact}}(x,t)}, \tag{42}$$

in which the variable y denotes $\eta(x,t)$ or $u(x,t)$.

Table 4
Relative errors in phase and amplitude.

n	m	$e^{\eta_0}_{\text{phase}}$	$e^{\eta_0}_{\text{amp}}$	$e^{u_0}_{\text{phase}}$	$e^{u_0}_{\text{amp}}$
500	1	0.100×10^{-3}	0.105×10^{-3}	0.314×10^{-4}	0.453×10^{-5}
1000	2	-0.893×10^{-5}	-0.119×10^{-5}	0.197×10^{-5}	0.284×10^{-6}
2000	3	0.107×10^{-5}	-0.194×10^{-6}	0.126×10^{-6}	0.181×10^{-7}
4000	4	-0.422×10^{-6}	0.921×10^{-7}	0.771×10^{-8}	0.109×10^{-8}

$\alpha = -0.39, \quad \delta = 0.3, \quad \hat{\mu} = 0.2, \quad \beta = 50, \quad \triangle x = 0.64/2^m, \quad t = 100, \quad A = -1.468564615,$

$C = 0.1066905917, \; x^{\text{exact}} = 40.66905917, \; \eta_0^{\text{exact}} = -5.363247863, \; u_0^{\text{exact}} = 7.876276033$

The constancy of the four invariants of motion derived in the previous section were monitored during the MOL computations, and the results are presented in Table (5) to illustrate the conservation properties of the numerical scheme.

The values of the invariants of motion were evaluated using accurate numerical integration and monitored at equal time intervals of 20. The numerical results for the four invariants I_1^{num}, I_2^{num}, I_3^{num} and , I_4^{num} remained constant to five significant digits for only 500 grid nodes. Such results are good indications that the numerical scheme has excellent conservation properties.

Table 5
Conservation of the invariants of motion.

Time	I_1^{num}	I_2^{num}	I_3^{num}	I_4^{num}
0	-0.49309×10^2	0.72413×10^2	-0.64119×10^3	-0.14868×10^3
20	-0.49309×10^2	0.72413×10^2	-0.64118×10^3	-0.14868×10^3
40	-0.49309×10^2	0.72413×10^2	-0.64119×10^3	-0.14868×10^3
60	-0.49309×10^2	0.72413×10^2	-0.64119×10^3	-0.14868×10^3
80	-0.49309×10^2	0.72413×10^2	-0.64119×10^3	-0.14867×10^3
100	-0.49309×10^2	0.72412×10^2	-0.64119×10^3	-0.14868×10^3

$\alpha = -0.39, \delta = 0.3, \hat{\mu} = 0.2, \beta = 50, \triangle x = 0.32, n = 500, \texttt{ATOL} = \texttt{RTOL} = 10^{-9}$

$A = -1.468564615, \; , C = 0.106690592, \; I_1^{\text{exact}} = -0.49309 \times 10^2,$

$I_2^{\text{exact}} = 0.72413 \times 10^2, \; I_3^{\text{exact}} = -0.64119 \times 10^3, \; I_4^{\text{exact}} = -0.14868 \times 10^3$

CONCLUSION

New exact solitary wave solutions for the Nwogu's one-dimensional extended Boussinesq equations were presented. New analytical expressions of four invariants of motions were also derived. A high order-accurate MOL was developed to compute solutions of the extended Boussinesq equations. The accuracy and conservative properties of the numerical scheme were assessed using the new exact solutions and analytical expressions of the constants of motion. Based on this experience and that of many previous studies (see Hamdi et al. [4] and Schiesser [12–14]), we conclude that the MOL may, with confidence, be used for the numerical integration of Boussinesq-Nwogu equations.

From a user stand point of view, our implementation of the MOL solution of the extended Boussinesq equations is simpler and straightforward compared to the numerical solutions of Walkley and Berzins [16] and Wei and Kirby [17]. There is no transformation or manipulation of the model equations. Our MOL implementation has the advantage of a close resemblance of the MOL programming of the the PDE with the PDE itself and uses a simple grid point ordering for bandwidth reduction of the Jacobian matrix of the integrator `DASSL`. This MOL implementation leads to efficient solutions of the Boussinesq system. The nonlinear terms and dispersive terms are accommodated easily using quality library routines [3,10,12–14].

A complete, documented FORTRAN code for the solution of Boussinesq-Nwogu equations, including all of the examples discussed in this papers, is available on request from the authors (email: samir.hamdi@utoronto.ca or wes1@lehigh.edu). This code can be easily modified to solve a wide range of Boussinesq-like equations with several applications in coastal engineering.

ACKNOWLEDGMENT

The financial support of the Natural Science and Engineering Research Council of Canada is gratefully acknowledged.

References

[1] Beji S, Nadaoka K. A formal derivation and numerical modeling of the improved Boussinesq equations for varying depth. *Coastal Engineering* 1996; **23**, 691–704.

[2] Brent RP. *Algorithms for minimization without derivatives*. Prentice Hall, Englewoods Cliffs:NJ, 1973.

[3] Fornberg B. Calculation of weights in finite difference formulas. *SIAM Review* 1998; **40**:(3): 685–691.

[4] Hamdi S, Gottlieb JJ, Hansen JS. Numerical solutions of the equal width wave equations using an adaptive method of lines. In *Adaptive Method of Lines,* Wouver AV, Saucez P,

Schiesser WE, (eds). Chapman & Hall/CRC Press: Boca Raton, Florida, 2001; 61–112.

[5] S. Hamdi, W.H. Enright, Y. Ouellet, W.E. Schiesser, Exact solutions of extended Boussinesq equations, accepted for publication in Numerical Algorithms, 2004.

[6] Lynett, P., and Liu, P. L.-F., A Two-Layer Approach to Water Wave Modeling, Proc. Royal Society of London A. v. 460, p. 2637-2669. 2004.

[7] Madsen PA, Murray R, Sørenson OR. A new form of the Boussinesq equations with improved linear dispersion characteristics. *Coastal Engineering* 1991; **15**: 371–388.

[8] Madsen PA, Sørenson OR. A new form of the Boussinesq equations with improved linear dispersion characteristics. Part 2. A slowly varying bathymetry. *Coastal Engineering* 1992; **18**: 183–204.

[9] Nwogu O. Alternative form of Boussinesq equations for nearshore wave propagation. *Journal of Waterway, Port, Coastal, and Ocean Engineering* 1993; **119**: 618–638.

[10] Petzold LR. A Description of DASSL: A differential/algebraic system solver. In *Scientific Computing*, Stepleman RS et (ed.). North Holland Publishing: Amsterdam, 1983.

[11] Schember HR. A new model for three-dimensional nonlinear dispersive long waves. PhD thesis, California Institute of Technology, Pasadena, California, 1982.

[12] Schiesser WE. *The Numerical Method of Lines Integration of Partial Differential Equations*. Academic Press: San Diego, 1991.

[13] Silebi CA, Schiesser WE. *Dynamic Modeling of Transport Process Systems*. Academic Press: San Diego, 1992.

[14] Schiesser WE. *Computational Mathematics in Engineering and Applied Science: ODEs, DAEs, and PDEs*. CRC Press: Boca Raton, Florida, 1994.

[15] M. Berzins, P.M. Dew and R.M. Furzeland, Developing software for time-dependent problems using the method of lines and differential-algebraic integrators , Appl. Numer. Math., 5, 375 397 (1989)

[16] Walkley M, Berzins M. A finite element method for the one-dimensional extended Boussinesq equations. *International Journal for Numerical Methods in Fluids* 1999; **29**: 143–157.

[17] Wei G, Kirby JT. Time-dependent numerical code for extended Boussinesq equations. *Journal of Waterway, Port, Coastal, and Ocean Engineering* 1995; **121**: 251–26.